nature photonics

ARTICLES

https://doi.org/10.1038/s41566-018-0174-8

Femtosecond laser crosslinking of the cornea for non-invasive vision correction

Chao Wang[1*], Mikhail Fomovsky[1], Guanxiong Miao[2], Mariya Zyablitskaya[3] and Sinisa Vukelic[1*]

The prevalence of myopia has increased worldwide over the last 50 years. Its incidence in the United States and Europe is now almost twice that 50 years ago, and it is even more prevalent in East Asia. Spectacles and contact lenses remain the most common means of vision correction, but the permanent correction of refractive errors, by refractive surgery, has emerged as an attractive alternative. However, such surgery is an invasive procedure that may compromise corneal structure, and post-surgical complications have been reported. We propose a novel, non-invasive approach to permanent vision correction based on a different mode of laser–cornea interaction. Our approach induces the formation of a low-density plasma that produces reactive oxygen species, which react with the surrounding proteins, forming crosslinks and triggering spatially resolved changes in mechanical properties. We show that the proposed method changes the refractive power of the eye, and confirm its safety and stability.

Myopia, or near-sightedness, is an eye condition in which incoming light is focused in front of, rather than on the retina. It is the most common refractive error and constitutes a growing public health problem worldwide. Its incidence has doubled over the last 50 years in the United States and Europe[1]. Myopia has also become an important issue in some East Asian countries, where its prevalence reaches 70 to 90%[2]. Most affected individuals use spectacles or contact lenses, which generally provide adequate refractive error correction. However, both are subject to limitations. Glasses do not work well in the rain and mist may form on them following changes in temperature or humidity. Contact lenses improve the field of vision and acuity, but many people find their presence on ocular surfaces intolerable[3]. Over the last 25 years, refractive surgery for the permanent correction of vision has thus emerged as an attractive choice for many patients[4]. Vision correction surgery, such as laser-assisted in situ keratomileusis (LASIK) and photorefractive keratectomy (PRK), reshapes the corneal curvature via laser-assisted ablation of a portion of the corneal tissue. These procedures are invasive and may weaken the cornea, leading to post-surgical complications. Furthermore, such procedures cannot be performed in a significant fraction of the population, due to the patient having a thin cornea, insufficient tear production or other abnormalities[4]. Efforts have been made to use riboflavin/ultraviolet (UV) light to correct myopia[5]. In such procedures, which were initially introduced for the treatment of keratoconus, corneas are soaked with riboflavin and then exposed to UV light to induce corneal crosslinking. However, this approach is suitable only in cases of weak myopia. We propose a novel, non-invasive approach to permanent vision correction through an innovative mode of laser–cornea interaction in which both thermal ablation[6] and optical breakdown[7] are avoided. Our approach is based on the induction of a low-density plasma (LDP)[8] to generate an ionization field within biological media without the production of damaging thermoacoustic[9] and shock waves[10]. When applied to collagenous tissues, LDPs induce the production of reactive oxygen species (ROS), which react with the surrounding proteins to form crosslinks and trigger spatially resolved changes in mechanical properties. We show here, with pig eyes ex vivo, that the proposed method effectively changes the refractive power of the eye. Follow-up experiments on rabbits in vivo confirmed its safety and stability. This method could expand the pool of patients eligible for permanent vision correction, while simultaneously eliminating the adverse effects associated with current forms of surgery. Furthermore, the approach described is also suitable for the treatment of keratoconus[11], and may have possible applications in other collagen-rich tissues, such as articular cartilage, in which it has been used to slow the progression of[12] early osteoarthritis.

Results and discussion

Laser-induced crosslink (CxL) formation alters the overall mechanical properties of the cornea, increasing its rigidity[11]. The concentration of laser energy achieved with this technique results in spatially resolved changes in mechanical properties, which are therefore controllable. This technique may be particularly useful for slowing or reversing keratoconus and post-LASIK ectasia. Furthermore, the treatment of specific volumetric regions of the corneal stroma leads to macroscopic changes in the overall corneal curvature (Fig. 1), which could be useful for the treatment of myopia, hyperopia, astigmatism and irregular astigmatism. Here, we present (1) an ex vivo study on pig eyes, providing a proof of principle for this technique, and (2) an in vivo study on rabbits, demonstrating the stability and safety of the induced changes. Pig eyes are frequently used in ophthalmic ex vivo research[13], and rabbits are widely used as a model for the correction of refractive errors[14].

Amending the effective refractive power of pig eyes ex vivo. We present two examples in the ex vivo study: corneal flattening, which is used to correct refractive errors due to myopia, and corneal steepening, which is used to treat hyperopia. We used a total of 60 fresh pig eyes for the study. Fifteen of these eyes underwent corneal flattening, and the treated eyes were paired with 10 control eyes. Thirteen eyes underwent laser irradiation to induce post-trea tment steepening; these eyes were also paired with 10 control eyes.

[1]Department of Mechanical Engineering, Columbia University, New York, NY, USA. [2]Department of Mechanical Engineering, Texas A&M University, College Station, TX, USA. [3]Department of Ophthalmology, Columbia University Medical Center, New York, NY, USA. *e-mail: chao.wang@columbia.edu; sv2147@columbia.edu

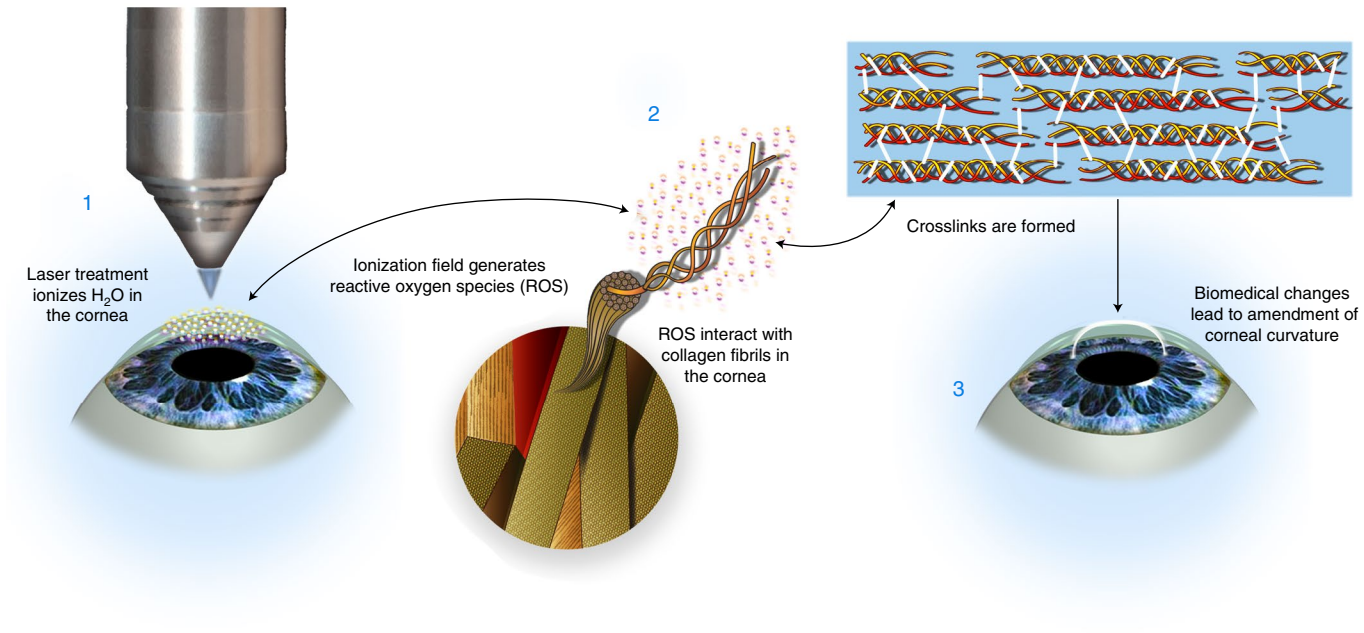

Fig. 1 | Step-by-step illustration of the use of the proposed laser-assisted process for the non-invasive correction of refractive errors .

The remaining 12 eyes were used for a separate control study, to evaluate the effects of the experimental set-up. For the flattening treatment (Fig. 2a) we treated a square in the middle of the eye. A strong change in corneal curvature, corresponding to a change in effective refractive power (ERP) of about 12% (a mean of about 5.11 dioptres), was initially observed, followed by partial recovery. Most of the change in curvature occurred within 8 h of treatment, after which the cornea stabilized at a refractive power of about 92% of the initial level (about 3.45 dioptres, on average). This significant change became evident when corneal topography before and after treatment was paired with the corresponding virtual vision findings, demonstrating the effects of the refractive error correction applied (topography and virtual vision are illustrated in the Supplementary Data). The initially large change in refractive power is due to a combination of the effects of the treatment itself and experimental conditions, including the temporary flattening of the cornea with a coverslip to ensure even volumetric exposure of the stroma to laser irradiation. The coverslip has an effect analogous to that of orthokeratology (ortho-K)[15], a temporary reshaping of the cornea used to reduce refractive errors, and the duration of the effect is similar to that of an ortho-K procedure. Once the effect of the coverslip wears off, the adjusted curvature remains stable throughout the rest of the 24 h period. By contrast, laser treatment of the peripheral zone of the cornea leads to its steepening (Fig. 2b). The ERP of pig eyes is significantly increased by treatment of a ring-shaped region. In the case of corneal steepening, the effective power of the eye increases gradually over a 12 h period, after which it stabilizes at a new value higher than that before treatment. This indicates that the induction of new CxLs counteracts the influence of the coverslip. For confirmation that the induced changes were photochemical in nature, and not due to thermal denaturation of collagen fibrils, we measured the laser-induced changes in corneal temperature. The relative change in temperature at the focal volume and in its immediate vicinity was less than 7 °C (for results see Supplementary Data). The heating induced by the treatment was thus well below the threshold for the thermal denaturation of collagen. Furthermore, examination under a light microscope equipped with Nomarski interference contrast optics revealed that there was no difference in refractive index between the treated and untreated parts of the cornea, consistent with an absence of corneal hazing (see Supplementary Data for further details).

The depth of the crosslinked region in the cornea was assessed by two-photon fluorescence (TPF) imaging. TPF imaging can be used to visualize changes induced in the cornea[16], because collagen is a primary extracellular source of nonlinear emissions[17]. The difference in structure between the control and treated regions of the cornea is shown in Fig. 3. This difference is due to the excitation of tyrosine and dityrosine oxidation products[17] and pyridinium-type fluorophores[18], strongly indicating that femtosecond laser treatment results in a significant increase in CxL density in the treated region[18,19].

These findings are consistent with reported results for the TPF imaging of glutaraldehyde-crosslinked collagen hydrogels[18] and riboflavin/UV light-crosslinked rabbit corneas[19]. The depth of the treated region was about 220 µm, consistent with the projected depth of treatment, suggesting that crosslinking does not decrease in efficiency as the focus of the laser pulses shifts toward the posterior stroma. Furthermore, crosslink density appeared to be fairly uniform throughout the treated volume, even though consecutive treatment planes were 50 µm apart.

In addition to evaluating changes in ERP and crosslink density, we also performed standard histological examinations of the pig corneas. No laser-induced damage was observed on haematoxylin and eosin (H&E) stained histological sections of corneas (for results see Supplementary Data). The pig corneas were also cultured for one week after treatment, to determine whether crosslink density remained stable, and to check for degradation in the crosslinked layers of the stromal matrix. Treatment delayed the injury-induced apoptosis of stromal keratocytes (for results and further discussion, see Supplementary Data).

In vivo studies in the rabbit model. Having obtained proof of principle in these initial ex vivo experiments on pig eyes, we then used the rabbit model to assess the stability of the changes in corneal curvature induced by laser treatment, and the safety of the procedure. A protocol almost identical to that used on pig eyes was applied to rabbit eyes in vivo, with a view to assessing changes in ERP after 24 h, seven days, and then weekly up to three months

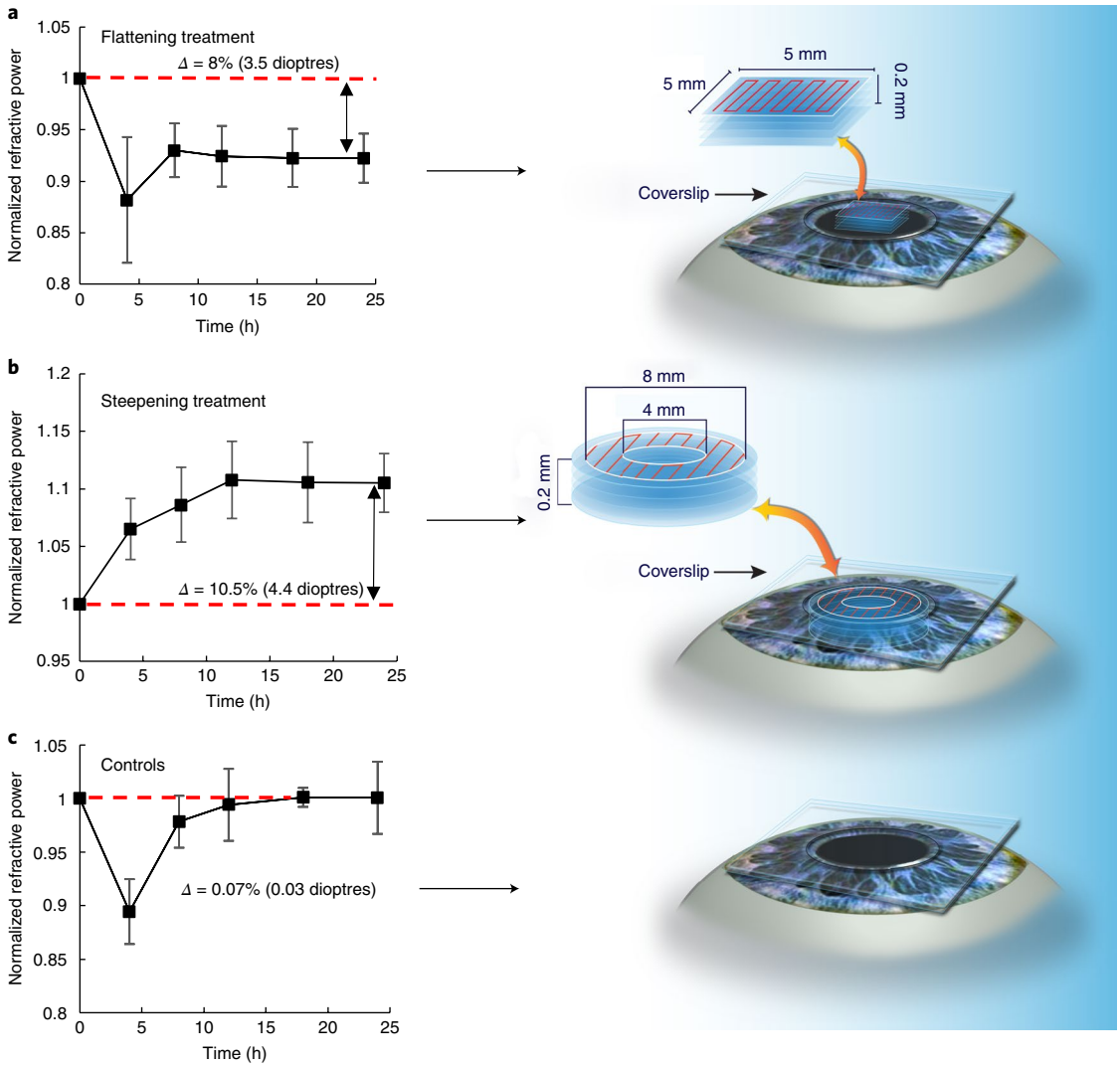

Fig. 2 | Laser-induced changes of the refractive power. a–c, Time course of the change in normalized ERP after laser treatment of pig eyes ex vivo and corresponding laser treatment: flattening (treatment of myopia) (**a**); steepening (treatment of hyperopia) (**b**); control study analysing the effects of the treatment protocol (**c**). The treatment involves applying laser pulses such that the path of the laser follows a zigzag trajectory, thus treating a planar area at a specific depth. The treatment is repeated at different depths, effectively inducing 'treatment layers'. Multiple treatment layers parallel to the surface were created, with a distance of 50 µm between consecutive planes. The *y* axis corresponds to ERP normalized against dioptre values before treatment. Changes in the refractive power of the eye relative to the measurement performed immediately before treatment are shown. Error bars indicate standard deviation. *Δ* indicates the change of ERP when compared with pretreatment values.

after treatment. Three groups of animals were assessed (for details of the groups, see Methods). In Group 1, the mean change in ERP 48 h after treatment was 1.74 dioptres (Fig. 4a) relative to the pre-treatment value. In Group 2, the change in ERP seven days after treatment was 1.64 dioptres (Fig. 4b). No significant change in ERP was observed in the control eyes of the rabbits of these two groups over these periods (Fig. 4a,b). The stability of the ERP changes induced by the treatment was monitored in the third group of animals (Fig. 4c). These changes remained stable for three months after treatment, with a relative change in ERP of about 1.94 dioptres for treated eyes.

The structure of H&E-stained histological sections of corneas obtained 48 h, one week and three months after treatment was similar to that of the control samples (Fig. 5). Specifically, no wound or wound-healing response resembling that observed after refractive surgery[14] was detected, and no collagen disorganization, epithelial cell and stromal oedema, intrastromal vacuole formation or endothelial cell detachment was observed; all these features are associated with thermal damage to stromal tissue, so we can thus conclude that no such damage occurred[20].

Confocal laser scanning microscopy (CLSM) images of rabbit eyes were obtained immediately after the rabbits had been killed (Groups 1 and 2) and in vivo (Group 3). The distance between two consecutive image planes was 2 µm for the epithelium and the stromal keratocyte network. The monolayer of endothelial cells was imaged separately. A comparison of CLSM images for intact rabbit eyes and laser-treated rabbit eyes revealed no significant difference in cellular structure and density (the CLSM images are presented in the Supplementary Data). Our CLSM images of the epithelial layer, stromal keratocyte network, and endothelium are similar to those obtained in other studies[21–23]. Our CLSM images of the endothelium (Supplementary Data) showed that cell shape and density were similar for treated eyes and their paired controls.

Low-density plasma produces ROS. The formation, by ROS, of intra- and intermolecular covalent bonds between collagen

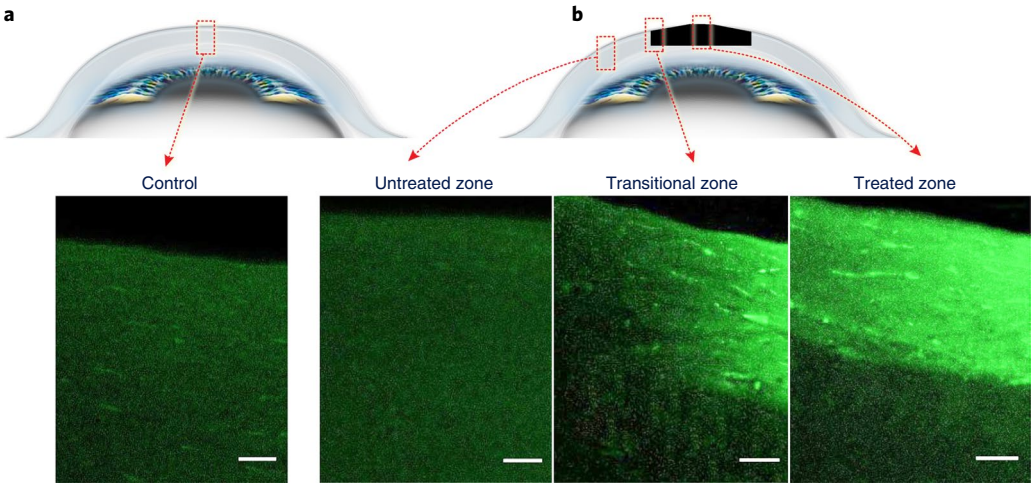

Fig. 3 | Differences in structure between control and laser-treated pig eyes. a,**b**, TPF images of cross-sections of control (**a**) and laser-treated (**b**) pig eyes. Three regions are imaged in the treated eye: an untreated region (left), a transitional region (middle) and the central region (right). Crosslink density is similar in the control sample and the untreated region of the laser-irradiated specimen. Scale bars, 60 μm.

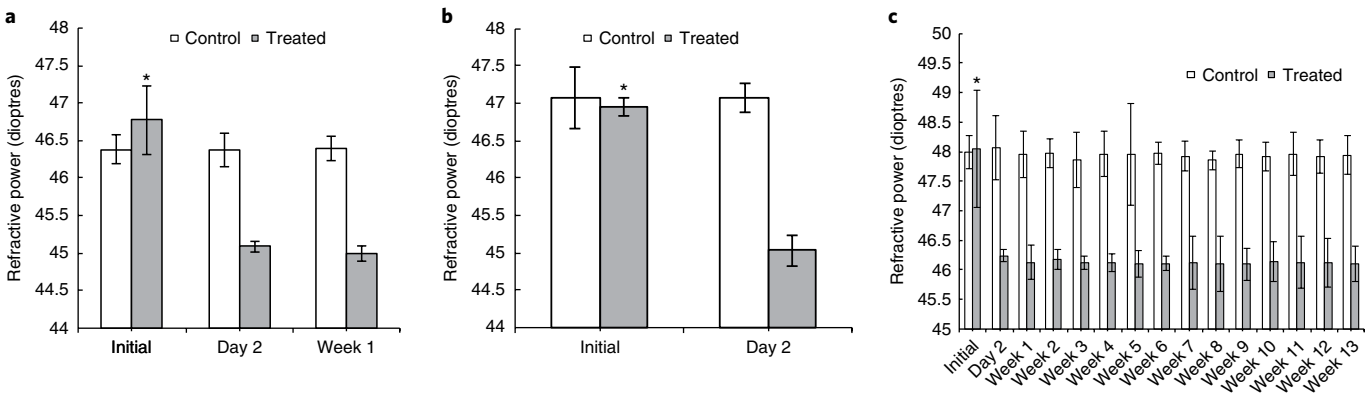

Fig. 4 | Time course of treatment-induced changes in the corneal ERP of live rabbits. a–**c**, Time course of changes for Group 1 (**a**), Group 2 (**b**) and Group 3 (**c**). ERP did not change in control eyes, whereas it decreased following laser treatment, subsequently remaining stable for three months after the procedure. *$P < 0.05$: statistically significant change in refractive power. Error bars indicate standard deviation.

fibrils has been observed following the exposure of riboflavin-soaked eyes to UVA light to initiate the crosslinking of corneal collagen for corneal stabilization in patients diagnosed with keratoconus[24]. However, ROS generation, as a by-product of plasma generation in aqueous media, has, itself, been the focus of considerable interest[25]. Free radical formation through two-photon ionization and the dissociation of water molecules was initially achieved by irradiation with high-power UV picosecond lasers[26]. Advances in femtosecond laser technology subsequently made phasing to multiphoton ionization (MPI) possible[25]. In aqueous environments, laser-induced ionization and dissociation occur as a cascade of reactions that can be classified as primary, secondary or tertiary. The primary reactions include the formation of solvated electrons and of the water cation radical, H_2O^+. This ROS is unstable and reacts with a water molecule to generate the H_3O^+ ion and the hydroxyl radical $OH^•$. The excited water molecule simultaneously dissociates, $H_2O^* \rightarrow H + OH^•$, generating another $OH^•$. The primary reactions are followed by secondary and tertiary reactions leading to the formation of H, O_2^-, OH^-, H_2, H_2O_2, HO_2 and other species[26].

The laser intensities used in studies focusing on ROS generation[25,26] were well above the irradiance threshold for femtosecond breakdown in aqueous and ocular media (~10^{13} W cm^{-2})[8], a level at which the density of free electrons released by photoionization reaches a critical value, resulting in the formation of a dense, optically opaque plasma[10]. However, as the number of free electrons produced during a single pulse is a function of irradiance, pulses generated by a femtosecond oscillator can be focused on aqueous or ocular media such that the density of laser-generated free electrons is well below the critical value for the formation of a dense plasma, but high enough for the generation of LDP[8]. In this situation, femtosecond irradiation is below the energy level required for optical breakdown, but atoms within the focal volume can be ionized, because the ionization probability has a number of resonance maxima due to the intermediate transition of the atom to an excited state[27]. In the vicinity of such maxima, the ionization cross-section increases by several orders of magnitude, making it possible for ionization to occur, even if the frequency of the incoming electromagnetic wave is below the ionization potential[27]. Multiple photons interact simultaneously with bound electrons to overcome the bandgap, producing an electron–hole pair[10,28]. Under these conditions, ionization of aqueous media is considered possible, and our hypothesis that the LDP produces ROS in aqueous solutions was confirmed by the use of electron paramagnetic resonance (EPR) spectroscopy to capture OH^- in an aqueous solution irradiated with a femtosecond oscillator (Fig. 6a).

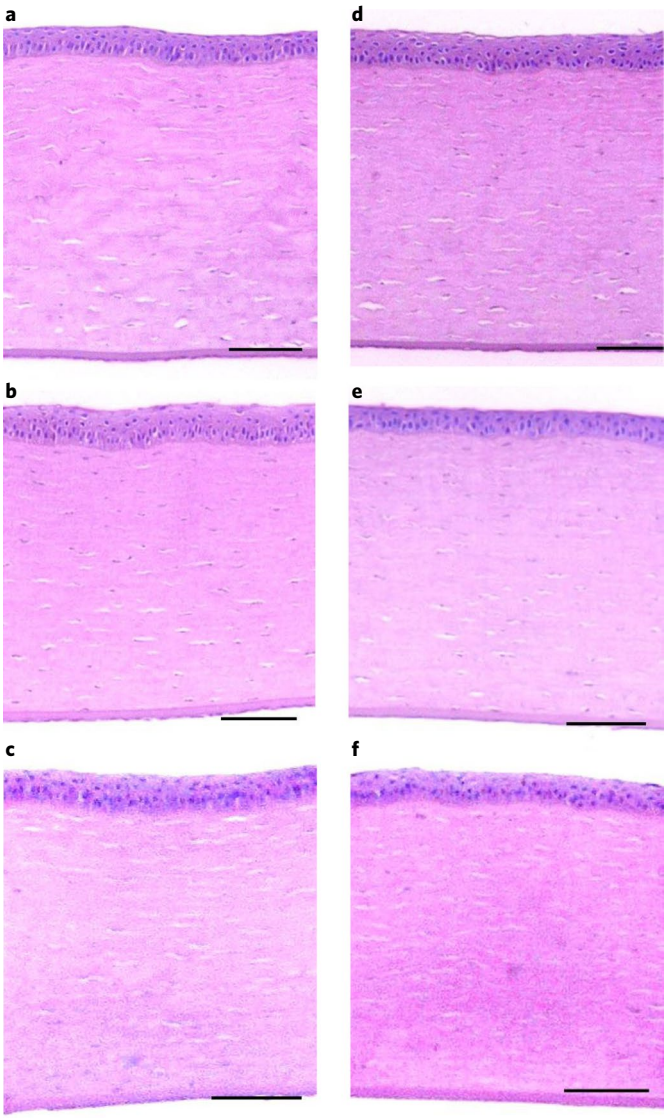

Fig. 5 | Histological sections of H&E-stained rabbit corneas. a–c, Sections taken two days after treatment (**a**); seven days after treatment (**b**); three months after treatment (**c**). **d–f**, Corresponding untreated controls. Scale bars, 100 µm.

Crosslink formation. ROS initiate the photo-oxidation of proteins, leading to the formation of chemical CxLs[29]. All amino acids are susceptible to modification by OH^- and $OH^- + O_2^-$ ($^+O_2$) radicals, but tryptophan, tyrosine, histidine and cysteine are particularly sensitive[30]. The amino acids involved in CxL formation in corneal tissue include histidine, hydroxylysine and tyrosine[31]. The oxidative modification of tyrosine is characterized by the abstraction of phenolic hydrogen atoms from tyrosine residues. The tyrosyl radical is relatively long-lived and can react with another tyrosyl radical or with tyrosine to form a stable, covalent carbon–carbon bond, resulting in the creation of 1,3-dityrosine[32]. The formation of this specific product of protein oxidation leads to intra- or intermolecular crosslinking[32] (Fig. 6b). This reaction primes pathways leading to crosslinking of the corneal stroma on irradiation with a femtosecond oscillator (Figs. 6c and 3). Furthermore, preliminary quantitative analyses of second-harmonic generation (SHG) images[33] (Fig. 6d) showed that CxLs locally increase the density of collagen structures in the anterior layers of the stroma, resulting in a homogeneous signal more regular than that of the untreated cornea. These changes directly influence overall corneal curvature, leading to changes in the refractive power of the eye. We performed a more detailed analysis of SHG images in a follow-up study[34].

Safety of the proposed procedure. The corneal stroma was crosslinked by the formation of free radicals, which have the potential to cause cell damage. For example, both in vitro[35] and in vivo[36] studies of the cytotoxicity of riboflavin/UVA procedures have shown that UV light-induced collagen crosslinking in the presence of riboflavin leads to an immediate loss of stromal keratocytes throughout the entire volume of the affected stroma. It can take up to six months to repopulate the corneal stroma with activated keratocytes[37], but this treatment is considered safe for humans unless the cornea is less than 400 µm thick. In such cases, the main safety concern is the potential for endothelial damage, as reported in both in vivo and in vitro studies[38,39]. The endothelium of the healthy cornea plays a key role in maintaining corneal hydration and transparency via active sodium–potassium adenosine triphosphatase (ATPase) and bicarbonate-dependent magnesium ATPase ion pumps. The corneal endothelial cells cannot replicate, and compensation can be achieved only by sliding[40]. If cell density decreases to levels below the critical limit, endothelial barrier dysfunction may occur, resulting in vision loss. Clinical studies have shown that corneas less than 400 µm thick in humans are susceptible to riboflavin/UVA treatment-related toxicity[41,42], and this has led to restrictions on the use of this technique. Our procedure is wavelength-independent, so an ultrafast laser operating in the infrared frequency domain can be used, avoiding the damaging effects of UV radiation. A quantitative analysis of keratocytes and endothelial cells with FIJI imaging software[43] showed that cell counts were similar in treated and control eyes. Keratocyte density 48 h after treatment ($39{,}464.29 \pm 2{,}288.57$ cells per mm^3) was similar to that in untreated controls ($39{,}523.82 \pm 5{,}868.68$ cells per mm^3). Keratocyte density remained stable for three months, in both treated and control eyes. Endothelial cell counts 48 h after treatment were $2{,}925.00 \pm 64.14$ cells per mm^2 for laser-irradiated corneas and $2{,}908.33 \pm 101.04$ cells per mm^2 for untreated controls. No change in endothelial cell density was observed seven days, one, two and three months after treatment (the quantitative analysis is summarized in Supplementary Fig. 5). The observed keratocyte and endothelial cell counts were within the normal range[44,45]. Confocal microscopy can reveal the presence of inflammatory cells in the cornea at an early stage of disease, before the appearance of external signs[46–48], but CLSM imaging showed that there was no inflammation-driven immune cell migration to the corneal stroma following laser treatment.

Conclusion

In this study, we used the LDP generated by a loosely focused femtosecond oscillator, a side effect of multiphoton imaging, to develop a method for treating ocular media. The proposed method, which exploits the nature of the interaction between ultrafast laser-generated LDP and collagenous tissue, can be used to induce CxLs in collagen-rich tissues without the use of photosensitizers, to modify the properties and geometry of these tissues. The novel laser–tissue interaction model described here was tested on pig eyes ex vivo and in rabbit models in vivo. It amended the refractive power of these eyes, suggesting that it could potentially be developed as a method for non-invasive vision correction. Selective alterations to the biochemical properties of pig and rabbit corneas improved refractive power. These changes in ERP remained stable for three months after treatment. Furthermore, histological and confocal imaging studies of the eyes revealed no signs of laser-induced damage, suggesting that the procedure is safe. Future studies will include the establishment of a mechanical model of the relationship between CxL density and the full-field deformation response of the corneal

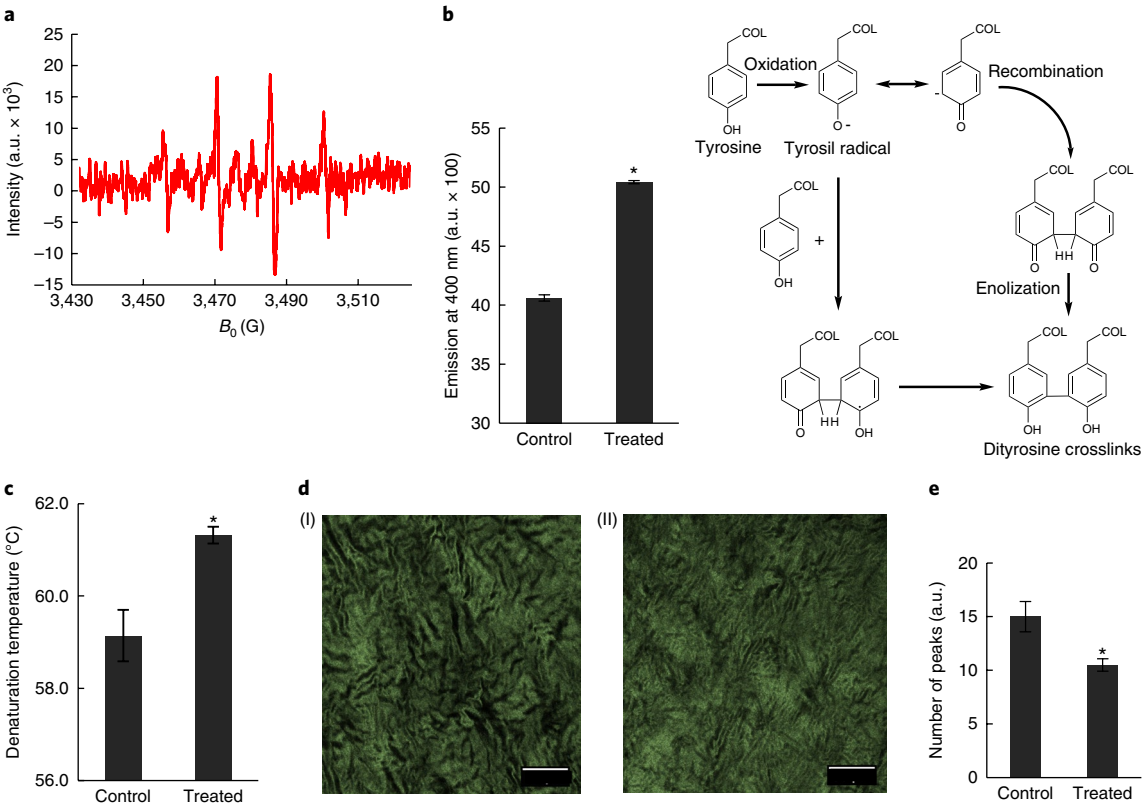

Fig. 6 | Mechanism of curvature adjustment. a, EPR spectrum demonstrating the $OH^{\bullet}$ and $O_2^{\bullet}$ generated by ionization of the solution with a femtosecond oscillator (low-density plasma ionizes the water in the cornea, forming ROS). **b**, Fluorescence spectra of laser-treated and control samples, and schematic diagram of the oxidative modification of tyrosine. Oxidative modifications of amino acids generates the tyrosyl radicals, and two tyrosyl radicals combine to form 1,3-dityrosine. **c**, Differential scanning calorimetry. ROS interaction with collagen results in crosslink formation. The thermal denaturation temperature of the treated corneal samples is about 2 °C higher than that for untreated samples. **d**, Second-harmonic generation (SHG) images of the anterior stroma of control (I) and laser-treated (II) pig eyes. CxLs locally increase the density of collagen structures in the anterior layers of the stroma, increasing homogeneity and resulting in a more regular signal pattern (II) than for untreated cornea (I). Scale bars, 50 µm. **e**, Bar chart showing the number of peaks above the cutoff line on the optical density plots for control and laser-treated corneas, used to quantify relative changes in the density of collagen structures in the corneal stroma[33]. *$P < 0.05$: statistically significant difference. Error bars indicate standard deviation.

stroma, as an understanding of the underlying corneal biomechanics is a prerequisite for the development of a clinically relevant technique. Finally, the laser–tissue model was applied exclusively to ocular media in this study, but the approach proposed could be extended to serve as a robust platform for use with other collagen-rich tissues requiring remodelling or an enhancement of mechanical properties.

Methods

Methods, including statements of data availability and any associated accession codes and references, are available at https://doi.org/10.1038/s41566-018-0174-8.

Received: 4 April 2017; Accepted: 12 April 2018;
Published online: 14 May 2018

References

1. Dolgin, E. The myopia boom. *Nature* **519**, 276–278 (2015).
2. Fredrick, D. R. Myopia. *Br. Med. J.* **324**, 1195–1199 (2002).
3. Richdale, K., Sinnott, L. T., Skadahl, E. & Nichols, J. J. Frequency of and factors associated with contact lens dissatisfaction and discontinuation. *Cornea* **26**, 168–174 (2007).
4. Solomon, K. D. et al. LASIK world literature review: quality of life and patient satisfaction. *Ophthalmology* **116**, 691–701 (2009).
5. Elling, M., Kersten-Gomez, I. & Dick, H. B. Photorefractive intrastromal corneal crosslinking for the treatment of myopic refractive errors: six-month interim findings. *J. Cataract Refract. Surg.* **43**, 789–795 (2017).
6. Gamaly, E. G., Rode, A. V., Luther-Davies, B. & Tikhonchuk, V. T. Ablation of solids by femtosecond lasers: ablation mechanism and ablation thresholds for metals and dielectrics. *Phys. Plasmas* **9**, 949–957 (2002).
7. Stuart, B. C. et al. Nanosecond-to-femtosecond laser-induced breakdown in dielectrics. *Phys. Rev. B Condens. Matter* **53**, 1749–1761 (1996).
8. Vogel, A., Noack, J., Hüttmann, G. & Paltauf, G. Low-density plasmas below the optical breakdown threshold: potential hazard for multiphoton microscopy, and a tool for the manipulation of intracellular events. *Proc. SPIE* **4620**, 202–216 (2002).
9. Vogel, A., Noack, J., Huttman, G. & Paltauf, G. Mechanisms of femtosecond laser nanosurgery of cells and tissues. *Appl. Phys. B Lasers Opt.* **81**, 1015–1047 (2005).
10. Schaffer, C. B., Jamison, A. O. & Mazur, E. Morphology of femtosecond laser-induced structural changes in bulk transparent materials. *Appl. Phys. Lett.* **84**, 1441–1443 (2004).
11. Guo, Y., Wang, C., Celi, N. & Vukelic, S. Femtosecond laser collagen cross-linking without traditional photosensitizers. *Proc. SPIE* **9321**, 932103 (2015).
12. Wang, C. et al. Femtosecond laser irradiation as novel paradigm for treatment of early osteoarthritis. In *Orthopaedic Research Society 2017 Annual Meeting* poster 563 (2017).
13. Wollensak, G., Spoerl, E. & Seiler, T. Stress–strain measurements of human and porcine corneas after riboflavin–ultraviolet-A-induced cross-linking. *J. Cataract Refract. Surg.* **29**, 1780–1785 (2003).
14. Heisterkamp, A. et al. Intrastromal refractive surgery with ultrashort laser pulses: in vivo study on the rabbit eye. *Graefes Arch. Clin. Exp. Ophthalmol.* **241**, 511–517 (2003).
15. Mountford, J, Ruston, D. & Dave, T. *Orthokeratology: Principles and Practice* (Butterworth-Heinemann, London, 2004).

16. Teng, S. W. et al. Multiphoton autofluorescence and second-harmonic generation imaging of the ex vivo porcine eye. *Invest. Ophthalmol. Vis. Sci.* **47**, 1216–1224 (2006).
17. Zipfel, W. R. et al. Live tissue intrinsic emission microscopy using multiphoton-excited native fluorescence and second harmonic generation. *Proc. Natl Acad. Sci. USA* **100**, 7075–7080 (2003).
18. Raub, C. B. et al. Noninvasive assessment of collagen gel microstructure and mechanics using multiphoton microscopy. *Biophys. J.* **92**, 2212–2222 (2007).
19. Steven, P., Hovakimyan, M., Guthoff, R. F., Huttmann, G. & Stachs, O. Imaging corneal crosslinking by autofluorescence 2-photon microscopy, second harmonic generation, and fluorescence lifetime measurements. *J. Cataract Refract. Surg.* **36**, 2150–2159 (2010).
20. Mencucci, R. et al. Ultrasound thermal damage to rabbit corneas after simulated phacoemulsification. *J. Cataract Refract. Surg.* **31**, 2180–2186 (2005).
21. Zyablitskaya, M. et al. Evaluation of therapeutic tissue crosslinking (TXL) for myopia using second harmonic generation signal microscopy in rabbit sclera. *Invest. Ophthalmol. Vis. Sci.* **58**, 21–29 (2017).
22. Zhang, W. et al. Rabbit model of corneal endothelial injury established using the Nd:YAG laser. *Cornea* **36**, 1274–1281 (2017).
23. Steven, P., Hovakimyan, M., Guthoff, R. F., Hüttmann, G. & Stachs, O. Imaging corneal crosslinking by autofluorescence 2-photon microscopy, second harmonic generation, and fluorescence lifetime measurements. *J. Cataract Refract. Surg.* **36**, 2150–2159 (2010).
24. Mastropasqua, L. Collagen cross-linking: when and how? A review of the state of the art of the technique and new perspectives. *Eye Vision* **2**, 19 (2015).
25. Migus, A., Gauduel, Y., Martin, J. L. & Antonetti, A. Excess electrons in liquid water: first evidence of a prehydrated state with femtosecond lifetime. *Phys. Rev. Lett.* **58**, 1559–1562 (1987).
26. Nikogosyan, D. N., Oraevsky, A. A. & Rupasov, V. I. Two-photon ionization and dissociation of liquid water by powerful laser UV radiation. *J. Chem. Phys.* **77**, 131–143 (1983).
27. Keldysh, L. Ionization in the field of a strong electromagnetic wave. *J. Exp. Theor. Phys.* **20**, 1307–1314 (1965).
28. Williams, F., Varma, S. & Hillenius, S. Liquid water as a lone-pair amorphous semiconductor. *J. Chem. Phys.* **64**, 1549–1554 (1976).
29. Kamaev, P., Friedman, M. D., Sherr, E. & Muller, D. Photochemical kinetics of corneal cross-linking with riboflavin. *Invest. Ophthalmol. Vis. Sci.* **53**, 2360–2367 (2012).
30. Davies, K., Delsignore, M. & Lin, S. Protein damage by oxygen radicals. II. Modification of amino acids. *J. Biol. Chem.* **262**, 9902–9907 (1987).
31. Meek, K. M. & Hayes, S. Corneal cross-linking—a review. *Ophthalmic Physiol. Opt.* **33**, 78–93 (2013).
32. Shen, H. R., Spikes, J. D., Smith, C. J. & Kopecek, J. Photodynamic cross-linking of proteins: V. Nature of the tyrosine–tyrosine bonds formed in the FMN-sensitized intermolecular cross-linking of *N*-acetyl-L-tyrosine. *J. Photochem. Photobiol.* **133**, 115–122 (2000).
33. Park, C. Y., Lee, J. K. & Chuck, R. S. Second harmonic generation imaging analysis of collagen arrangement in human cornea. *Invest. Ophthalmol. Vis. Sci.* **56**, 5622–5629 (2015).
34. Wang, C. et al. A new paradigm for use of utrafast lasers in ophthalmology for enhancement of corneal mechanical properties and permanent correction of refractive errors. *Proc. SPIE* **10066**, 100660Y (2017).
35. del Buey, M. A., Lanchares, E., Cristóbal, J. Á., Gotor, C. Y. & Calvo, B. Immediate effect of ultraviolet-A collagen cross-linking therapy on the biomechanics and histology of the human cornea. *J. Refract. Surg.* **31**, 70–71 (2015).
36. Alhayek, A. & Lu, P. R. Corneal collagen crosslinking in keratoconus and other eye disease. *Int. J. Ophthalmol.* **8**, 407 (2015).
37. Mazzotta, C. et al. Treatment of progressive keratoconus by riboflavin-UVA-induced cross-linking of corneal collagen: ultrastructural analysis by Heidelberg Retinal Tomograph II in vivo confocal microscopy in humans. *Cornea* **26**, 390–397 (2007).
38. Wollensak, G., Iomdina, E., Dittert, D. D. & Herbst, H. Wound healing in the rabbit cornea after corneal collagen cross-linking with riboflavin and UVA. *Cornea* **26**, 600–605 (2007).
39. Wollensak, G., Spoerl, E., Wilsch, M. & Seiler, T. Endothelial cell damage after riboflavin–ultraviolet-A treatment in the rabbit. *J. Cataract Refract. Surg.* **29**, 1786–1790 (2003).
40. Kim, S., Cha, D., Song, Y. B., Choi, J. Y. & Han, Y. K. Effects of senofilcon A mechanical protector on corneal endothelial cells during phacoemulsification in rabbit eyes: pilot study. *J. Cataract Refract. Surg.* **43**, 394–399 (2017).
41. Kymionis, G. D. et al. Corneal collagen cross-linking with riboflavin and ultraviolet-A irradiation in patients with thin corneas. *Am. J. Ophthalmol.* **153**, 24–28 (2012).
42. Spoerl, E., Mrochen, M., Sliney, D., Trokel, S. & Seiler, T. Safety of UVA–riboflavin cross-linking of the cornea. *Cornea* **26**, 385–389 (2007).
43. Schindelin, J. et al. Fiji: an open-source platform for biological-image analysis. *Nat. Methods* **9**, 676–682 (2012).
44. Petroll, W. M., Boettcher, K., Barry, P., Cavanagh, H. D. & Jester, J. V. Quantitative assessment of anteroposterior keratocyte density in the normal rabbit cornea. *Cornea* **14**, 3–9 (1995).
45. Twa, M. D. & Giese, M. J. Assessment of corneal thickness and keratocyte density in a rabbit model of laser in situ keratomileusis using scanning laser confocal microscopy. *Am. J. Ophthalmol.* **152**, 941–953 (2011).
46. Liang, H. et al. In vivo confocal microscopy and ex vivo flow cytometry: new tools for assessing ocular inflammation applied to rabbit lipopolysaccharide-induced conjunctivitis. *Mol. Vis.* **12**, 1392–1402 (2006).
47. Mantopoulos, D., Cruzat, A. & Hamrah, P. *Semin. Ophthalmol.* **25**, 178–185 (2010).
48. Lagali, N. et al. *Confocal Laser Microscopy—Principles and Applications in Medicine, Biology, and the Food Sciences* (InTech Open Limited, London, 2013).

Acknowledgements

This research was partly funded by the Wallace H. Coulter Foundation. The authors thank S. Trokel for helpful discussions and comments on the manuscript, D. Paik for allowing us to use the equipment in his laboratory, J. Yu, F. Ji, C. Diao and J. Fan for assisting with laser treatment, the experimental set-up and figure preparation, D. Bian for performing the refractive index measurements, and W.D.A.M. De Boer and W. Yang for running TPF experiments. The authors also thank S. Jockusch for help with running EPR spectroscopy experiments. The authors acknowledge Fundação para a Ciência e Tecnologia (FCT) projects PTDC/SAU-ENB/122128/2010 and PEST-C/SAU/UI3282/2013 and COMPETE programmes FCOMP-01-0124-FEDER-021163 and FCOMP-01-0124-FEDER-037299 for support for the multiphoton microscopy equipment. The authors thank JenLab GmbH for providing the required equipment and A. Kaiser for transporting the pig eyes.

Author contributions

C.W. and S.V. designed the ex vivo and in vivo treatments, as well as tissue culturing studies. C.W. performed these experiments. M.F., G.M. and M.Z. assisted C.W. with the characterization. M.F. and S.V. designed the ROS trapping experiment, tyrosine crosslinking and SHG analysis of treated corneal tissue. M.F. performed the experiments, and C.W. assisted. M.Z. performed the in vivo CLSM measurements, and C.W. analysed them. C.W. and G.M. built the experimental set-up. S.V. initiated, designed and supervised the project. C.W., M.F. and S.V. wrote the manuscript.

Competing interests

The authors declare no competing interests.

Additional information

Supplementary information is available for this paper at https://doi.org/10.1038/s41566-018-0174-8.

Reprints and permissions information is available at www.nature.com/reprints.

Correspondence and requests for materials should be addressed to C.W. or S.V.

Publisher's note: Springer Nature remains neutral with regard to jurisdictional claims in published maps and institutional affiliations.

Methods

Ex vivo eye treatment. Pairs of fresh pig eyes were recovered from an abattoir (Green Village Packing), less than 2 h after the animals had been killed. They were placed on ice and immediately transported to the laboratory. We used 60 pig eyes in total. Fifteen eyes were subjected to flattening treatment. The treated eyes were paired with 10 control eyes. Thirteen eyes underwent laser irradiation to demonstrate post-treatment steepening. These eyes were also paired with 10 control eyes. The remaining 12 eyes were used for a separate control study, to evaluate the effects of the experimental set-up. Excess tissue was removed from the isolated eyes, which were then rinsed with Dulbecco's phosphate-buffered saline (DPBS, 1×, Sigma-Aldrich) and brought to room temperature in a damp chamber. The eyes were examined and any defective samples were discarded. The epithelial layer of the retained specimens was removed by gentle scraping with a 10 mm scalpel blade[49] and the eye globes were mounted on a custom-built eye holder (see Supplementary Data for a schematic diagram). The epithelial layer was removed to ensure consistency between the specimens, as most had experienced superficial damage during handling at the abattoir. Intraocular pressure was maintained (~16 mmHg) by connecting an intravenous (i.v.) system filled with 0.9% NaCl solution (Hospira) to the eyeball via a 22G needle (BD). A customized digital pressure gauge with an Omega PX154 low-differential pressure transmitter was used to adjust the pressure. Immediately before treatment, the corneal surface was covered with a microscope coverslip (#1 Microscope Cover Glasses, VWR International) to ensure homogeneous volumetric irradiation of the cornea. An Nd:glass femtosecond oscillator (High Q Laser) was used to generate laser pulses with a temporal pulse width of 99 fs and a repetition rate of 52.06 MHz, at a wavelength of 1,059.2 nm. A Zeiss Plan Neofluar ×40 objective lens with a numerical aperture (NA) of 0.6 was used to focus the beam, and the mean power of the laser system after the objective lens was 60 mW. The samples were mounted on a three-axis motorized PT1 translational stage powered by Z825B motorized actuators (Thorlabs). The treatment consisted of laser pulses applied by moving the stage in an x–y plane, such that the laser path followed a zigzag trajectory at a feed rate of 2.2 mm s^{-1}, resulting in treatment of a planar area at a specific depth. The objective focused the laser on a spot of about 2 µm in diameter. There was therefore a spot overlap of about 90%. The treatment was repeated at different depths, resulting in 'treatment layers'. Multiple treatment layers were created parallel to the surface, with a distance of 50 µm between consecutive planes, giving an effective depth of treatment of about 200 µm. The laser beam was focused on the anterior cornea, from the corneal surface to a depth of up to 200 µm. With every 'treatment layer', the laser was focused exclusively on the cornea, ensuring that the lens was not damaged. The flattening treatment took about 37 min, whereas corneal steepening took about 90 min to complete under the conditions described. The experimental set-up is shown in the Supplementary Data, and schematic diagrams of the treatment paths are provided in the main text (Fig. 2). A paired control eye was subjected to a protocol identical to that used for the treated eyes, and was mounted on the same stage while the other eye was being treated, but was not itself exposed to the laser. The coverslip was carefully removed immediately after treatment. During the 24 h characterization period, we applied 3 ml of PBS to each eye at 20 min intervals to stop the eyes drying out.

Animals. In vivo experiments were performed on young adult Dutch belted rabbits, each weighing 1.8–2.0 kg. Rabbits are commonly used as models for the correction of refractive errors, despite anatomic differences between human and rabbit eyes, such as the higher regenerative capacity of the endothelial layer[50] and doubts about the possible presence of a Bowman's layer in rabbits[14]. The animals were delivered to the Columbia University Institute of Comparative Medicine (ICM) animal house one week before laser treatment, to allow the animals time to get used to their new environment. The experimental protocol and pre- and post-treatment handling procedures were reviewed and approved by the Institutional Animal Care and Use Committee of Columbia University. The 12 animals used in the study were assigned to three groups. The animals in the first group ($n=3$) were euthanized and their eyes were removed 48 h after laser treatment, to investigate the acute effects of laser irradiation. The animals in the second group ($n=3$) were euthanized after one week, to allow the eyes to undergo at least partial healing if the laser had damaged the tissue. In this group, the refractive power of the eye was also determined 48 h after treatment. The last group of animals ($n=6$) was monitored to investigate the long-term stability of the induced changes in refractive power. Half of the animals in the last group were euthanized after three months, to determine whether there was any treatment-induced damage or other morphological changes. The animals were euthanized 48 h (Group 1), seven days (Group 2) and three months (half the animals in Group 3) after treatment by i.v. injection of pentobarbital (100 mg kg^{-1}) into the marginal ear vein. The cornea, retina and lens were isolated, fixed by incubation with 10% formalin overnight, desorbed by incubation with 70% alcohol for 24 h, and sent to Columbia Medical Center Histology Service for histological staining. The samples were embedded in paraffin wax and cut into 5-µm-thick cross-sections, which were then stained with H&E. These sections were observed with a VHX 5000 digital microscope (Keyence Corporation), and the acquired images were processed with ImageJ software[51,52].

In vivo eye treatment. Before treatment, the animal corneas were subjected to macroscopic examination and slit-lamp evaluation by a veterinary surgeon to ensure that there were no abnormalities or eye injuries. The rabbits were anaesthetized with an intramuscular injection of ketamine (3.5 mg kg^{-1}) and xylazine (5 mg kg^{-1}), placed on a warm heating pad, and monitored until fully unconscious. The depth of anaesthesia was confirmed by the absence of pedal and ear-pinch reflexes[53]. Anaesthetized rabbits were gently placed on their sides in a custom-built, heavily padded holder for immobilization (see Supplementary Fig. 2a,b). The eye facing upwards was treated, and the eye facing downwards was used as the untreated control. Proparacaine (0.5% ophthalmic solution) drops were applied to the treated eye for local anaesthesia, followed by GenTeal water-based gel (Novartis, Alcon) to prevent corneal dehydration. GenTeal gel was applied to both eyes and replenished during the procedure, as required. The treated eye was gently pressed with a coverslip to ensure the homogeneous volumetric application of laser pulses. The laser treatment protocol was based on the procedure developed on porcine eyes ex vivo, as described above. However, the laser beam (Nd:glass ultrafast laser, Hi-Q Laser), focused via an objective with high NA (Zeiss, Plan Neofluar ×40/0.6 NA) on the desired volumetric zone of the cornea, was delivered to the rabbit eye by mounting the objective on a custom-built three-axis motion system with three translational stages (PT1, Thorlabs) coupled to motorized actuators (Z825B, Thorlabs). A number of optical components, including mirrors and lenses, were mounted on the motion system to steer the laser beam into the back aperture of the objective. As in the ex vivo study, laser pulses were rasterized by moving the objective in an x–y plane such that the laser beam followed a zigzag trajectory, resulting in treatment of a circular planar area (diameter of 5 mm) at a specific depth (Supplementary Fig. 2c). Again, as in the ex vivo study, the treatment was repeated at different depths to generate treatment layers. Five treatment layers parallel to the surface were created, with a distance of 50 µm between consecutive layers. This treatment resulted in corneal flattening (Fig. 4). The rabbits were returned to the ICM animal facility immediately after treatment.

Ex vivo corneal topography characterization. We used an EyeSys Vision clinical eye topography characterization instrument (EyeSys System 2000, EyeSys Vision) with version 1.50 software to capture corneal topography and calculate the ERP immediately before treatment, and after laser irradiation. Measurements were made at regular intervals over a 24 h period after treatment of the eyes. During this characterization, the corneal surface was moistened with Systane Ultra Lubricant Eye Drops (Novartis). Following application of an eye drop, the eye holder was moved gently in a circular motion to distribute the lubricant evenly over the ocular surface and allow any excess lubricant to slide off the eye. The topography of a pig eye before and after treatment is shown in the Supplementary Data. Topographic results are paired with virtual vision results to demonstrate the effects of the laser treatment.

In vivo topographic measurements. Topographic measurements were performed with an Eyesys Vision non-contact eye-topographer (EyeSys Vision)[54,55]. Topographic measurements of the entire corneal area were performed before treatment, 48 h after treatment (Groups 1, 2 and 3), seven days after treatment (Groups 2 and 3), and then once weekly (Group 3) to assess the effects of laser light-induced corneal crosslinking on potential changes in the refractive power of the eye. Corneal topography measurements were also made immediately after treatment. Highly irregular patterns and abnormal results were observed in some cases due to an anaesthesia-driven drop in intraocular pressure; these results were excluded from the analysis.

TPF microscopy. In total, eight freshly collected corneal samples, four from control eyes and four from treated eyes, were cut into 2 mm^2 blocks with a custom-built slicer, mounted in a 3 mm Petri dish and processed for TPF microscopy. We used a two-photon microscope (Bruker), with a Mai Tai Deep See Ti:sapphire laser (Spectra Physics) as the excitation source. A ×40/0.8 NA water immersion objective (Olympus) was used to acquire the fluorescence signals, which were registered with two different photomultiplier tubes, one in the red (580–620 nm) and the other in the green (480–570 nm) wavelengths of visible light. The excitation wavelength was 826 nm. The green channel was used for data acquisition. Measurements were processed with ImageJ software.

CLSM. Cellular evaluations of corneal tissues were performed by CLSM imaging with an HRT3-RCM laser scanning system (670 nm laser beam, Heidelberg Engineering) equipped with a ×63/0.95 NA water immersion objective (Zeiss). Imaging was performed immediately after death for the rabbits of Group 1 (48 h after treatment) and Group 2 (7 days after treatment) and in vivo for Group 3 (one, two and three months after treatment). A disposable sterile plastic cap was placed on the objective to maintain the distance between the corneal surface and the objective. The animals were placed in a custom-built holder during the process, with the eyelids of the imaged eye gently pulled open by hand. GenTeal water-based gel was applied as a coupling medium. The entire corneal volume was scanned and recorded, with optical sections through the epithelium, stroma and endothelium[48,56].

EPR spectroscopy. EPR spectroscopy was performed on laser-irradiated DPBS. The radicals produced by the laser irradiation of DPBS were captured with the spin-trapping reagent 5,5-dimethyl-1-pyrroline-*N*-oxide (DMPO, Cayman Chemicals). DMPO was dissolved in DPBS, at a final concentration of 100 mM. We added 170 µl of the sample to a shallow dish (2 × 8 mm) covered with a microscope coverslip. The dish was then placed on a three-axis motorized stage for laser treatment. A control sample was prepared in parallel, with the same procedures. Immediately after treatment, as described in the eye treatment sections, both treated and control solutions were collected into 0.5 ml tubes, which were then placed in a canister of liquid nitrogen for transport to the EPR spectrometer (Bruker BioSpin EMX Electron Paramagnetic Resonance Spectrometer, Bruker BioSpin) for characterization. The total time from sample treatment to EPR analysis was less than 15 min in all cases.

Fluorospectrometric detection of dityrosine. We prepared 5 mM L-tyrosine (Sigma-Aldrich) in Tris buffer pH 10. Samples were placed in shallow 170 µl dishes, covered with a microscope coverslip, and treated with a femtosecond oscillator, as described in the eye treatment sections. After laser irradiation, the samples were transferred to a black 96-well plate (Thermo Fisher Scientific) and their fluorescence was measured with excitation at 325 nm and emission at 400 nm (ref. [57]) on a Gen5 Microplate Reader (BioTeK Instruments). Untreated L-tyrosine solution was subjected to the same procedure, under identical conditions, as a control.

DSC. Corneal punches (5 mm in diameter) were extracted from laser-treated and untreated corneal samples, sealed in plastic film to stop the tissues from drying out and stored frozen at −20 °C. The punch samples were thawed immediately before characterization, rinsed in DPBS, and blotted on a paper towel folded in half to remove excess solution. Samples weighing about 26 mg were sealed in 50 µl aluminium pans (Perkin-Elmer Universal Crimper Press) and loaded into the DSC autosampler (Perkin-Elmer DSC 6000 autosampler) for measurement of denaturation temperature. Samples were characterized as described elsewhere[58]. Briefly, they were heated to temperatures of 40–70 °C at a speed of 18 °C min^{-1}. Denaturation curves representing differential heat flow over time were generated (see Supplementary Fig. 6 and brief discussion in the Supplementary Data) and analysed with Pyris (version 11.0).

SHG microscopy. Corneas were collected immediately after laser irradiation of the eyes. They were fixed by incubation overnight in 4% paraformaldehyde at 5 °C. After fixation, 2 mm^2 blocks were dissected from the central region, washed in PBS, mounted in 50% glycerol in PBS on microscope coverslips and imaged. The sample preparation process has been described in detail elsewhere[59]. The second harmonic signal was generated with a laser (Chameleon Vision II, Coherent) tuned to 850 nm on an A1RMP laser scanning system mounted on an Eclipse TiE microscope stand (Nikon Instruments) equipped with a ×25/1.1 NA ApoLWD water-immersion objective. The back-scatter configuration was used to acquire the SHG signal with the non-descanned detector (Nikon) and a 400–450 nm bandpass filter. The microscope was controlled with NIS Elements software (Nikon). The images acquired were analysed as described in a previous study[33]. The images were preprocessed with the spatial frequency filter. We used set-ups with 100 and 20 pixels to analyse large and small features, respectively. After initial processing, the images were converted to binary signals and plotted. The optical density of the black and white areas on the binary images was assessed by determining the number of peaks crossing the median cutoff intensity. The crossing densities measured at the vertical midline are considered to represent the complexity (irregularity) of collagen structure patterns: the higher the crossing density, the more complex the collagen bundle pattern. Crossing density is therefore used here as a surrogate for pattern irregularity[33]. SHG imaging and analysis were performed on the central regions of anterior corneas. Groups of laser-treated and control samples were prepared for SHG imaging, with each group containing four corneas.

Temperature measurements. For temperature measurements, fresh ex vivo pig eyes were placed in a customized holder under the three-axis motorized femtosecond laser head. The conditions for laser treatment were as described in the eye treatment sections. The corneal tissue was moistened with PBS before measurement. The needle-like tip of a customized thermocouple (Omega Single Strand, Insulated Thermocouple Wire, diameter of 0.07 mm, temperature measurement range 0–100 °C) was inserted into the middle of the cornea, parallel to the surface. Real-time temperature readings were displayed on a computer equipped with a LabView temperature input module (National Instruments Cooperation LabView Student Edition 2016). The focal point was carefully aligned with the tip of the thermocouple, and the temperature distribution was measured as the focal volume was moved laterally away from the tip of the thermocouple (see Supplementary Fig. 7a for a schematic diagram of the procedure). Three eyes were used for characterization, and 14 measurements were performed per eye. Each consecutive temperature measurement was made along a testing line 18° away from the previous measurement, in the same plane.

Refractive index measurements. Nomarski interference contrast characterization was performed on the corneas with an Olympus BX 60 fluorescence microscope (Olympus) equipped with a ×20/0.45 PLAN APO objective (Olympus), 24 h after treatment. A Nomarski interference contrast (refractive index sensitivity of about 0.08) prism was used to enhance the contrast between regions of the cornea with potentially different refractive indices. Before the examination, corneas were fixed by incubation in 10% formalin overnight, followed by desorption in 70% alcohol for 24 h.

Data availability. The data used for the plots shown in this paper and other findings of the study are available from the corresponding authors upon reasonable request.

References

49. Gupta, P. et al. Depth resolved differences after corneal crosslinking with and without epithelial debridement using multimodal imaging. *Transl. Vis. Sci. Technol.* **3**, 5 (2014).
50. Van Horn, D. L., Sendele, D. D., Seideman, S. & Buco, P. J. Regenerative capacity of the corneal endothelium in rabbit and cat. *Invest. Ophthalmol. Vis. Sci.* **16**, 597–613 (1977).
51. Wollensak, G. & Iomdina, E. Biomechanical and histological changes after corneal crosslinking with and without epithelial debridement. *J. Cataract Refract. Surg.* **35**, 540–546 (2009).
52. Davis, F. A. The anatomy and histology of the eye and orbit of the rabbit. *Trans. Am. Ophthalmol. Soc.* **27**, 400–402 (1929).
53. Zhang, Z.-Y. et al. Refractive change in the adult rabbit eye after corneal relaxation with the femtosecond laser. *BMC Ophthalmol.* **14**, 8 (2014).
54. Fagerholm, P. Wound healing after photorefractive keratectomy. *J. Cataract Refract. Surg.* **26**, 432–447 (2000).
55. Shojaei, A. et al. Short-time mitomycin-C application during photorefractive keratectomy in patients with low myopia. *J. Cataract Refract. Surg.* **39**, 197–203 (2013).
56. Zhivov, A., Stachs, O., Stave, J. & Guthoff, R. F. In vivo three-dimensional confocal laser scanning microscopy of corneal surface and epithelium. *Br. J. Ophthalmol.* **93**, 667–672 (2009).
57. Dalle-Donne, I., Milzani, A. & Colombo, R. Fluorometric detection of dityrosine coupled with HPLC separation for determining actin oxidation. *Am. Biotechnol. Lab.* **19**, 34–39 (2001).
58. Takaoka, A. et al. An evaluation of lysyl oxidase-derived cross-linking in keratoconus by liquid chromatography/mass spectrometry. *Invest. Ophthalmol. Vis. Sci.* **57**, 126–136 (2016).
59. Morishige, N. et al. Quantitative analysis of collagen lamellae in the normal and keratoconic human cornea by second harmonic generation imaging microscopy. *Invest. Ophthalmol. Vis. Sci.* **55**, 8377–8385 (2014).